Catalysis Today 301 (2018) 226–238

Contents lists available at ScienceDirect

Catalysis Today

journal homepage: www.elsevier.com/locate/cattod

Synthesis of Pd-Al/biomorphic carbon catalysts using cellulose as carbon precursor

F. Cazaña[a], A. Galetti[b], C. Meyer[a,1], V. Sebastián[a], M.A. Centeno[c], E. Romeo[a], A. Monzón[a,*]

[a] Departamento de Ingeniería Química y Tecnologías del Medio Ambiente, Instituto de Nanociencia de Aragón (INA), Universidad de Zaragoza, 50018 Zaragoza, Spain
[b] Instituto de Investigaciones en Tecnología Química (INTEQUI-CONICET-UNSL), Chacabuco y Pedernera, 5700 San Luis, Argentina
[c] Instituto de Ciencia de Materiales de Sevilla, Centro Mixto CSIC-Universidad de Sevilla, 41092 Sevilla, Spain

ARTICLE INFO

Keywords:
Biomorphic catalyst
Pd
Carbon support
Cellulose
Cyclohexene hydrogenation

ABSTRACT

This work presents the results obtained with novel Pd and Pd-Al catalysts supported on carbon, which have been prepared using a biomorphic mineralization technique. The catalyst synthesis procedure includes a stage of thermal decomposition under reductive atmosphere of cellulose previously impregnated with the metallic precursors. We have studied the influence of the temperature and time of decomposition, and of the Al precursor addition, on the textural and catalytic properties. The characterisation results indicate that the preparation method used leads to the formation of carbonaceous supports with a high microporosity (up to 97% micropore volume) and values of the BET surface up to 470 m^2/g while maintaining the original external structure. The use of low temperatures (ca. 600 °C) during the decomposition step allows the preparation of highly dispersed catalysts with narrow Pd particle size distributions. However, the thermal decomposition at elevated temperatures (ca. 800 °C) increases the Pd particle size due to the sintering of the metallic phase. This phenomenon is augmented with the decomposition time and is not affected by the presence of Al. Consequently, the catalytic activity of these materials in cyclohexene hydrogenation is strongly affected by the operational conditions used during the thermal decomposition step. Unexpectedly, the more sintered catalysts, i.e. those prepared at 800 °C, show the highest activity. According to the characterization results, this fact can be explained considering that the smaller Pd particles obtained after preparation at e.g. 600 °C are quite inactive because they are confined in the internal structure of the micropores of the support and/or embedded inside the carbon matrix. In contrast, after decomposition at 800 °C, the larger Pd particles formed are placed at the external surface of the catalyst, being accessible to the reactants. In addition, for the specific conditions under which the Pd is accessible, the presence of Al favours the cyclohexene conversion due to the enhancement of the adsorption on the Pd surface as a consequence of a charge transfer phenomenon. These results can serve as a guideline for the preparation of these catalysts based on raw lignocellulosic materials in order to maximize their catalytic performance.

1. Introduction

Biomorphic carbon materials produced by controlled carbonization of lignocellulosic biomass wastes, or of various other biological resources, are promising materials for many practical applications. In most cases, biomorphic carbon materials have been investigated as electrodes in energy accumulator systems, due to their large and electrochemically stable surface and high electrical conductivity. In addition, their interconnected porous structure with controllable pore sizes make these materials very suitable for the transport of electrolyte ions and reacting molecules [1,2]. Because of these properties, this type of carbon is also widely used as filtration membranes and as adsorbents for air and water purification. Other fields of research include electrochemical hydrogen storage [3], or the development of thermal insulating materials [4]. Of course, the above-mentioned properties related to the chemical stability and controllable porous structure make biomorphic carbons excellent potential supports for catalysts in liquid or gas phase reactions [5–7].

Usually, this type of carbon is prepared by mineralization of the raw material. This technology allows the synthesis of inorganic materials using biological structures as templates [8,9]. This technique can be used to prepare materials whose production is very difficult using other

* Corresponding author.
E-mail address: amonzon@unizar.es (A. Monzón).
[1] On leave from INCAPE (UNL-CONICET), Santa Fe, Argentina.

http://dx.doi.org/10.1016/j.cattod.2017.05.026
Received 4 December 2016; Received in revised form 30 March 2017; Accepted 5 May 2017
Available online 11 May 2017
0920-5861/

methods such as the “top-down” or “self-assembly” processes [10].

Some materials of natural origin, as for example vegetable tissues, have complex structures [8,11,12,13–15,16] that when reproduced with inorganic materials can be used in a wide range of applications such as catalysis, photonics, filters, drug delivery, molecular electronics, etc [15]. Plant constituents have high stiffness and elasticity at the micro and at the macro-scale, excellent resistance at low density and an anisotropic porous morphology [17,18]. All the above features make these materials very attractive for use in the development of new structured systems such as structured catalytic rectors, membranes, etc. [19].

Biomorphic materials are generally prepared by reactive or by molding techniques. Reactive techniques involve the pyrolysis of a bio-organic template into biomorphic material, in an inert or reducing atmosphere. In addition, before the pyrolysis, the raw material can be impregnated with catalytic precursors (e.g. Ni, Cu, Pd, Au, Si, Al, etc). In this case, after the thermal decomposition step, the solid obtained is made up of a biomorphic carbonaceous support containing highly dispersed metallic nanoparticles. Using this technique, supported metallic catalysts can be easily synthesized with a structure replicating original bio-organic material. The main limitation of this technique is that the use of high temperatures can destroy a large part of the original nanostructure with the result that the replication is only achieved at the microstructure but not at the nanostructure level [15]. On the other hand, the technique known as *chemical templating* allows the developing of materials in which the nanostructure of original materials is replicated perfectly. This technique is considerably more complex and involves a process in which the plant cells suffer chemical modifications (e.g. acid treatments), followed by the infiltration of precursor sols. Silica or iron oxide replicas of the cell wall structure can be developed with this technique [20,21].

In this work, a series of Pd and Pd-Al supported biomorphic carbon catalysts has been developed through reactive techniques because this is easier and cheaper than using the chemical templating protocols. In order to know how the thermal decomposition temperature and the addition of Al affect the physicochemical properties of these catalysts, the synthesized samples were characterized by thermogravimetric analyses in air (TGA-Air), nitrogen adsorption isotherm, Raman spectroscopy, X-Ray diffraction (XRD), X-Ray photoelectron spectroscopy (XPS), scanning electron microscopy (SEM) and transmission electron microscopy (TEM). The activity of the prepared catalysts was measured in the liquid phase cyclohexene hydrogenation reaction, because this does not present any problem of selectivity and stability under the reaction conditions. The results obtained were compared with a typical catalyst of Pd/SiO_2, in order to know if the biomorphic carbons are suitable for use as catalytic supports in liquid phase reactions.

2. Experimental

2.1. Materials

The organic material used to prepare the biomorphic catalyst was cellulose provided by Sigma Aldrich. The metal precursors were Pd (II) nitrate hydrate supplied by Acros Organics (ref.: 10239293) and Al nitrate nonahydrate provided by Sigma Aldrich (ref.: 237973). Al oxide (98%) and silica gel (refs.: 11028 and 60741, respectively), used as catalyst model supports, were supplied by Sigma Aldrich. The solvent selected for the reaction was decalin (decahydronaphtalene) and the reactive was cyclohexene, both purchased from Sigma Aldrich (refs.: 294772 and 125431, respectively).

2.2. Catalysts preparation

The catalysts were prepared with 6% of Pd and variable contents of Al: 0%, 1.75% and 7%. These were named respectively as: Pd/BC, Pd-Al (1.75)/BC and Pd-Al(7)/BC and were prepared in the following manner. The cellulose was dried at 100 °C overnight and then impregnated by incipient wetness with the appropriate amounts and concentrations of Pd and Al aqueous solutions. After impregnation, the solid was dried at 80 °C overnight and then thermally decomposed in a reducing atmosphere (15% H_2, 85% N_2). The temperature and time of the thermal decomposition stage was varied from 600 °C to 800 °C and from 30 to 120 min, respectively. In all cases, the decomposition temperature was reached at high heating rates (ca. 42 °C/min). Finally, the catalyst was milled and sieved to obtain a homogeneous particle size distribution ranging between 80 and 200 micrometres.

The comparison catalyst of $Pd(1\%)/SiO_2$ was also prepared by the incipient wetness method. The support, SiO_2, was impregnated by a Pd aqueous solution, dried at 100 °C overnight, and finally calcined at 300 °C for 3 h in air. The final catalysts were milled to obtain a homogeneous particle size ranging between 80 and 140 micrometres.

2.3. Catalytic conversion of cyclohexene

The catalytic hydrogenation of cyclohexene was carried out in a high pressure reactor (Berhof BR-100) following a procedure similar to that described previously [6]. Briefly, 20 mg of the selected catalyst was added to a vessel containing 32.5 mL of decalin. With the aim of attaining high dispersion of the catalyst particles, the mixture was sonicated for 15 min at 25% amplitude in an Ultrasonic Processor 750 W, and then placed in the reactor. In order to avoid the presence of any re-oxidized layer of Pd at the surface of the exposed particles, the catalyst was reduced *in situ* at 100 °C and 20 bar pressure of hydrogen for 1 h. After that, a solution containing 3.8 mL of cyclohexene and 1.2 mL of decalin was added to the reactor. The temperature and hydrogen pressure were then kept at 100 °C and 20 bar, respectively, during the reaction. A stirring rate of 1400 rpm was selected after checking that under these operating conditions the external and internal mass-transfer limitations are negligible. After 1 h reaction time, the hydrogen was evacuated from the reactor and nitrogen was introduced to maintain an inert atmosphere during the cooling step. The reactor was cooled in an ice bath to room temperature. The reactor content was then filtered and the liquid phase analysed by a GC Agilent 7890A equipped with a J & W HP-5 capillary column and FID detector. The integration of the peaks, corresponding to cyclohexene, cyclohexane and decalin, displayed in the chromatogram was used to calculate the conversion of cyclohexene.

2.4. Catalyst characterization

The catalysts were characterized by several techniques in order to ascertain the textural and structural properties. The thermogravimetric analyses in air (TGA-Air) were carried out using a Mettler Toledo TGA/SDTA 851e. The air flux used during the TGA measurements was 50 mL/min. This technique was employed to calculate the amount of Pd and Al deposited on the biomorphic carbon support after the thermal decomposition of the cellulose. After the decomposition step in TGA-Air, the solid residue of the catalysts contained ashes, PdO and, in the case of the samples with Al, Al_2O_3. The percentage of ashes was calculated from metal-free biomorphic carbon prepared under the same experimental conditions as the catalysts. The Pd content was estimated as the difference between the Pd/BC residue and the ashes previously calculated. In the same way, the Al content was estimated subtracting the Pd content and the ashes from the Pd-Al/BC residue. In order to check the validity of this method, an Al(7%)/BC sample was also synthesised, and the concordance of the% of Al was excellent. The protocol was repeated three times with each sample, obtaining in all cases coefficients of variation less than 2%.

Specific area and porosity were obtained from nitrogen adsorption–desorption isotherms at 77 K using an ASAP 2020 (Micromeritics Instrument Corp.). BET specific surface areas were measured from the adsorption branches in the relative pressure range of 0.001–0.10.

Mesopore size distributions were calculated using the *NLDFT Carbon Slit Pores* model, while micropore size distributions were calculated using the *Horvath-Kawazoe* (H-K) model. The micropore volume estimation was made by means of the *Dubinin-Radushkevich* method [22].

The X-ray diffraction (XRD) patterns were recorded within the range of 5–90° (2θ) using Rigaku/Max Cu rotatory anode equipment operating at 40 kv and 80 mA with Cu K_α radiation. The X-Ray photoelectron spectroscopy (XPS) patterns were obtained using Kratos Axis ULTRA equipment with Al K_α radiation.

Transmission electron microscopy (TEM) micrograph images were recorded by a FEI Tecnai T-20 microscope, operated at 200 kV. On the other hand, STEM-HAADF images were acquired with a FEI Tecnai F-30 microscope, coupled with an EDS detector, operated at 300 kV. Scanning electron microscopy (SEM) micrograph images were captured by a FEI Inspect F50 microscope, operated at 10 kV.

Biomorphic carbon was characterized by Raman spectroscopy to ascertain the content of carbon defects and graphitic carbon in each sample. The Raman spectra were measured through 532 nm laser excitation using a WiTec Alpha300 Confocal Raman Microscope.

3. Results and discussion

3.1. Catalysts characterization

Fig. 1 shows the TGA-DTG curves for the carbon prepared from cellulose and for the Pd/BC and Pd-Al(7)/BC catalysts. The combustion occurs in the temperature interval between 470 °C and 650 °C, similarly to that obtained by Xie et al. when studying carbons derived from cellulose and lignin [23]. In the case of the BC derived from cellulose, the combustion peak appears at ca. 620 °C while for the samples containing Pd and Pd-Al the corresponding peaks appear at lower temperatures, 480 °C and 520 °C respectively, due to the catalytic effect of Pd during the combustion [24]. For the case of the Pd/BC sample, in the interval from 600 °C to 1000 °C the mass remains constant, corresponding to the solid residue composed of ashes and PdO [25]. The curve corresponding to the Pd-Al(7)/BC catalyst shows an initial loss of mass of about 10% (from room temperature to 400 °C). This initial mass loss could indicate that the pseudo-boehmite (or a partially hydrated or hidroxilated alumina), obtained during the catalyst preparation by decomposition of the Al nitrate, is transformed into γ-Al_2O_3 at the temperatures attained in the TGA-DTG experiment. Therefore, in this case, the amount of remaining material after oxidation corresponds to PdO, γ-Al_2O_3 and minor amounts of ashes. Table 1 compares the nominal compositions of Pd and Al, based on the initial amount of cellulose, and the final content of these metals on the final biomorphic carbon support, calculated from the TGA-air data of all the samples prepared. Replicated TGA measurements indicate that the values of metal composition calculated with this method have variations lower than 3%, indicating the validity of this procedure. Due to the loss of carbonaceous material during the thermal decomposition stage, the weight percentage of Pd and Al is markedly increased in the final catalysts compared to the initial amount on the raw cellulose. In addition, Table also includes the bulk atomic ratios for the Pd/BC and Pd-Al/BC samples.

Table 1
Pd and Al contents (atomic%) of the catalysts.[a]

Catalyst	% weight on cellulose		% weight on BC		Atomic Ratios		
	Pd	Al	Pd	Al	10^3·Pd/C	10^3·Al/C	Pd/Al
Pd/BC	1.00	–	6.11	–	7.34	0.00	
Pd-Al (1.75)/ BC	1.00	0.50	6.27	1.75	7.69	7.88	0.98
Pd-Al(7)/ BC	1.00	2.00	6.31	6.98	8.21	33.4	0.25

[a] Decomposition time = 30 min at 800 °C.

The final Pd content is about 6% (wt%), and the Al contents are 0, 1.75% and 7% respectively. In this regard, the development of new preparation methods of carbon supported catalysts with high metallic phase contents is an important issue in the fields of fuel cell electrodes or electro-catalysis [26,27]. In these cases, the electrodes need to have elevated contents of Pt (at least 40 wt%) with a high dispersion in order to obtain high charge densities. Therefore, the preparation method proposed here could be used as an alternative procedure to produce these kinds of catalytic materials.

The textural effects of the thermal treatment conditions and of the Al addition were investigated by N_2 adsorption. Fig. 2 shows the N_2 adsorption/desorption isotherms for the Pd/BC and Pd-Al(7)/BC catalysts prepared using a thermal treatment of 30 min at 800 °C. According

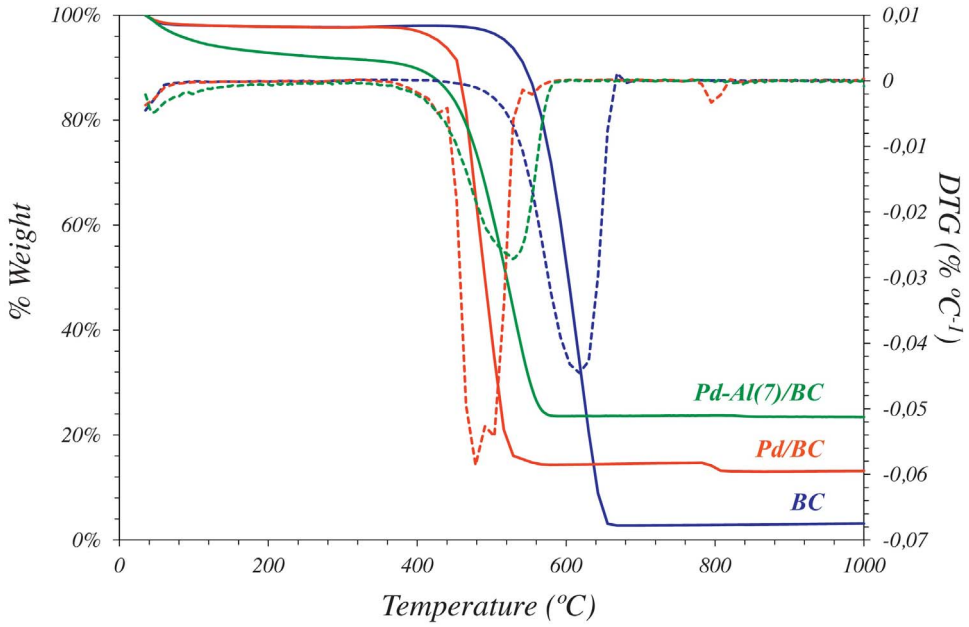

Fig. 1. TGA-Air analyses for biomorphic carbon, Pd/BC and Pd-Al(7)/BC catalysts prepared at 800 °C during 30 min.

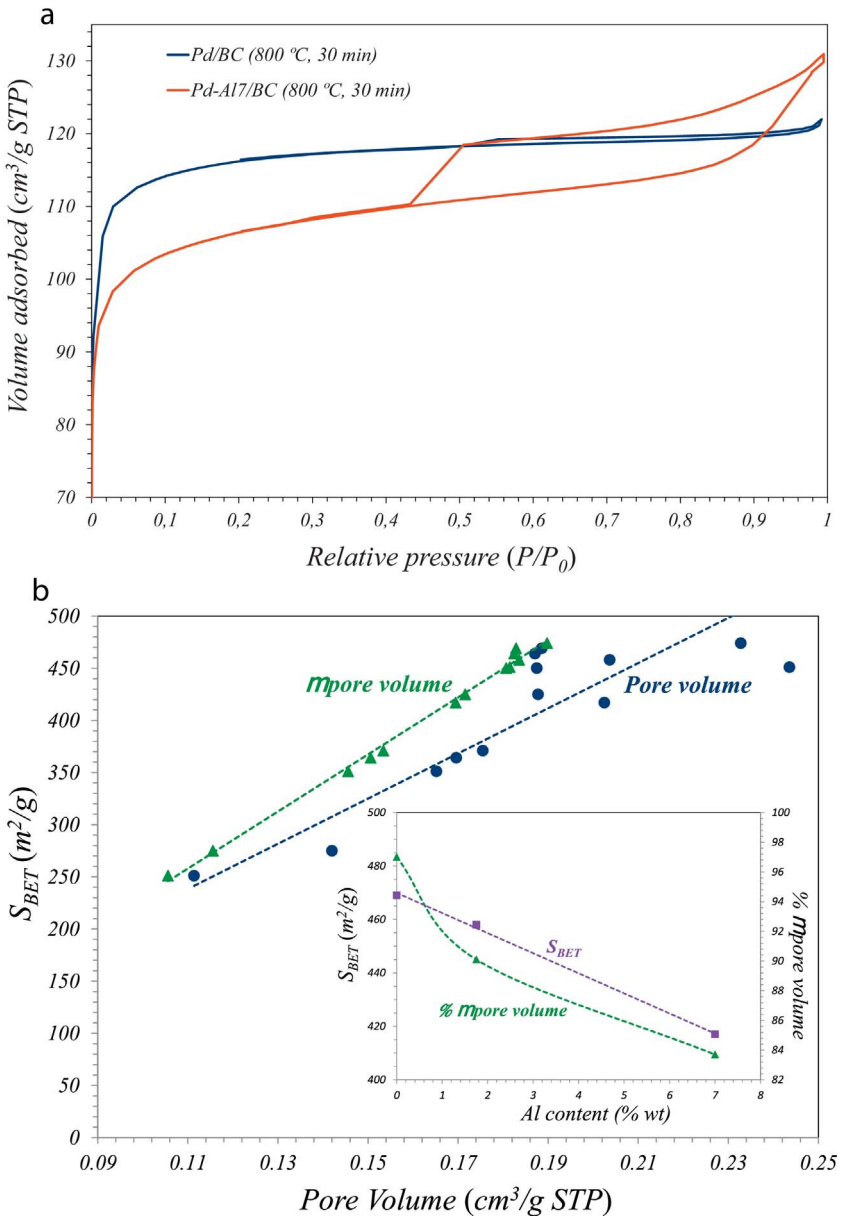

Fig. 2. a) N_2 adsorption and desorption isotherm for Pd/BC and Pd-Al(7)/BC decomposed at 800 °C during 30 min. b) BET surface area vs. the pore volume (blue circles), and micropore volume (green triangles). Insert: S_{BET} and% μpore volume vs.% Al. (For interpretation of the references to color in this figure legend, the reader is referred to the web version of this article.)

to the IUPAC classification, in the first case the isotherm corresponds to the II-type with a hysteresis loop of type H3 or H4 [28,29]. These types of hysteresis loops are typical of disordered materials with distributions of pores size and ill-defined shapes [29]. In the case of the Pd-Al(7)/BC, it is clear that the addition of Al modifies the adsorption results, exhibiting now a broader hysteresis loop of type H3 or H4, and increasing the mesoporosity. This result is also corroborated by the *NLDFT Carbon Slit Pores* model calculations [29].

In addition, Table 2 shows the values of the BET surface area, total pore volume, micropore volume and micropore diameter as a function of the temperature and time used during the thermal decomposition step. For the case of the Pd/BC catalyst, there is almost no change of specific surface area and pore volume when varying the decomposition temperature (see Table 2).

The influence of the Al addition can be compared for the samples prepared at 800 °C during 30 min. In this case, the BET area decreases from 469 m^2/g for the Pd/BC sample to 458 m^2/g after the addition of 1.75% of Al, and to 417 m^2/g for the Pd-Al(7)/BC catalyst. Similarly, for the Pd-Al(7)/BC sample, the increase from 600 °C to 800 °C during the preparation increases the BET area, the total pore volume and of the micropore volume, but decreases the% of the micropore volume. The catalysts prepared at 600 °C and 800 °C present a maximum for the BET surface at 75 min, while the BET surface increases continuously with the preparation time for the sample obtained at 700 °C. In contrast, the % micropore volume exhibits a maximum at 75 min for the catalysts prepared at 600 °C and 700 °C, whereas the sample prepared at 800 °C shows a decrease in the% of the micropore volume. In the latter case, the partial blockage of the pores is due to the formation of large Pd particles (> 60 nm) at 800 °C (see XRD and TEM results).

This complex pattern of the relationship between the textural properties of the synthesized materials and the preparation conditions are rationalized in the representation in Fig. 2b of the values of the BET surface area vs. the pore volume (blue circles) and the micropore volume (green triangles). As shown in this Figure and in the data in Table 3, there is a clear linear correlation between the BET surface area and the micropore volume of the sample, especially in the case of the

Table 2
Textural properties of the catalysts. Influence of temperature and time of thermal decomposition.

Catalysts	Temperature (°C)	Time (min)	BET surface (m^2/g)	Pore volume (cm^3/g)	Micropore volume (cm^3/g)	% Micropores	$d_{\mu p}$ (nm)
Pd/BC	600	30	450	0.1875	0.1807	96.4	0.50
	700	30	464	0.1871	0.1825	97.5	0.53
	800	30	469	0.1886	0.1829	97.0	0.52
Pd-Al(1.75)/BC	800	30	458	0.2037	0.1836	90.1	0.50
Pd-Al(7)/BC	600	30	275	0.1420	0.1156	81.4	0.56
	600	75	364	0.1696	0.1506	88.8	0.55
	600	120	251	0.1114	0.1056	94.5	0.56
	700	30	351	0.1652	0.1456	88.1	0.56
	700	75	371	0.1755	0.1534	87.4	0.50
	700	120	425	0.1878	0.1716	91.4	0.42
	800	30	417	0.2025	0.1695	83.7	0.53
	800	75	474	0.2328	0.1898	81.5	0.51
	800	120	451	0.2436	0.1815	74.5	0.51

Table 3
Linear correlations of Pore volume vs. S_{BET} data in Fig. 2b.

	All data	Pd-Al	Pd
μpore volume			
R^2	0,995	0,999	0,993
Slope (m^2/cm^3)	2752,6	2659,2	8373,8
pore volume			
R^2	0,724	0,896	0,247
Slope (m^2/cm^3)	1888,3	1803,0	6298,3

Pd-Al samples (R^2 = 0.99875), confirming that the most relevant textural parameter for these materials is the micropore volume. Moreover, the slope of the straight line corresponding to the Pd-Al samples is 2659.2 m^2/cm^3, which is highly consistent with the result obtained by Scherdel et al. [30]. These authors obtained a value of 2559 m^2/cm^3 using samples of synthetic carbons derived from porous resins pyrolyzed at 800 °C in Argon, and then exposed to temperatures ranging from 1000 °C to 2500 °C in an inert argon atmosphere [31,32].

For the calculation of the micropore volume we have used the Dubinin-Radushkevich model [22], which is the common approach used for the characterization of microporous carbons [29]. On the other hand, the BET-method was developed for the study of the surface adsorption on meso- and macroporous solids [29,33], and therefore the linear relationship obtained in Fig. 2b would not be expected. However, as pointed out previously [30,34,35], the results in Tables 2 and 3 and in Fig. 2b indicate that the BET model can also be applicable for microporous samples. In the present case, given that the greater part of the pore volume (ca. 90%) is in the microporous range; inevitably, the BET surface area measurements must include the adsorption in the micropores. The decrease in the correlation between the S_{BET} with the total pore volume is caused by the samples with a lower% of micropores, in which the increase in the pore volume does not cause an increase in the surface area. Thus, in the case of the samples Pd-Al (7)/BC prepared at 800 °C during 75 and 120 min (the last two rows in Table 2), the% of micropores is markedly lower due also to the large size of the majority of the metallic Pd nanoparticles generated by the sintering produced over such long thermal decomposition times during the catalyst preparation. Thus, for the samples decomposed during 30 min, the insert in Fig. 2b shows the almost linear decrease in the BET area and the% of the micro-pore volume with the Al content. This result is consistent with the assumption that, after 30 min of thermal treatment, the amount of aluminium added to the sample is mainly responsible for the evolution of the textural properties. For a given Al content, the increase in the duration of the treatment, e.g. up to 120 min, increases the Pd size, causing an additional loss of the% of microporosity (see Table 2).

Fig. 3 shows the XRD patterns of the Pd/BC catalysts prepared at 600, 700 and 800 °C, and of the Pd-Al catalysts prepared at 800 °C. In all the cases studied, the peaks obtained correspond only to metallic Pd. There are no peaks associated to PdO. The broad peak obtained at around 24 ° corresponds to the plane (002) of the carbonaceous material formed after the decomposition step, and indicates that at the temperatures attained during the preparation, the crystalline domains of the carbonaceous support are too small to be visible by XRD.

The sharpening of the Pd peak increases with the decomposition temperature, indicating an increase in the Pd crystallite size. This is consistent with the TEM measurements, also shown in Table 4, where the excellent correlation between the values obtained using XRD and TEM measurements can be seen. The absence of peaks related to the alumina indicates that the specie formed is poorly crystallized in the form of small particles at the surface of the support.

Using the Scherrer equation, the crystallite sizes calculated for the Pd/BC at 600, 700 and 800 °C are 5.8, 12.5 and 30.1 nm, respectively. As expected, the increase in the preparation temperature causes substantial sintering of the metallic phase and, accordingly, a decrease in the Pd dispersion from 15% to 3.1% (see Table 7). The presence of Al in the catalyst composition does not modify the Pd size. For a given preparation temperature, the increase in the decomposition time intensifies the sintering phenomenon. Thus, after 120 min at 800 °C, the average Pd size attains a value of around 66 nm (see Table 4), and the Pd dispersion falls to less than 2% (Table 7).

Table 5 shows the XPS results obtained for C, O, Pd and Al for the samples prepared varying the decomposition temperature and the Al content. It can be observed that for the Pd/BC sample, the oxygen content slightly increases with the temperature of decomposition, from 7.57% at 600 °C to 8.64% at 800 °C. As expected in the presence of Al, the% of oxygen on the surface increased up to 16%, due to the formation of aluminum oxide during the decomposition stage.

Furthermore, the spectra corresponding to the signal of oxygen (O 1s) and of C (C 1s), (not shown) include the contributions of several functional groups of C and O. Thus, the C spectra can be deconvolved in a first peak at 284.9 eV, corresponding to sp^2/sp^3 carbon, a second peak at 286.1 eV, corresponding to the C−O bond, a third peak at 286.8 eV, corresponding to the C═O bond and a fourth peak at 288.9 eV, corresponding to O−C═O groups [36]. From these deconvolutions it has been estimated that around 24% of the carbon at the surface is linked to oxygen, forming −C−O, −C═O or −O−C═O groups. The most abundant organic functional groups are the carboxilic groups (ca. 46%) and the rest have similar contents (ca. 27% of both −C−O and −C═O groups).

As regards the Pd content, it was found that around 7.5% of the surface Pd particles were oxidised. The catalyst pre-reduction step before the reaction eliminates this oxide layer and activates the exposed Pd nanoparticles.

Although the XRD and TEM results (see Table 4 and Fig. 7) clearly indicate that the Pd particle sizes increase with the thermal decomposition temperature, the increase in the Pd/C ratio from $7.74.10^{-3}$ at

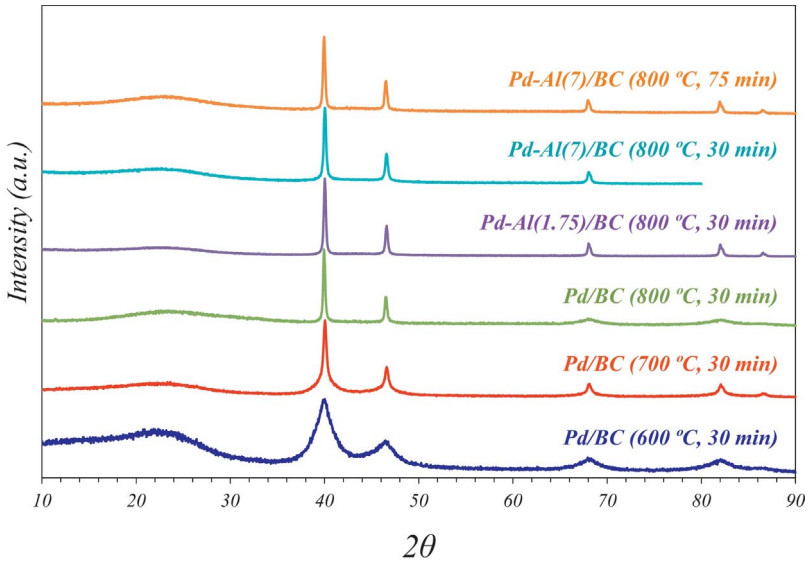

Fig. 3. XRD pattern obtained for prepared catalysts. Influence of thermal decomposition temperature and aluminium addition.

600 °C to $8.83.10^{-3}$ at 800 °C observed for the Pd/BC samples indicates that, as the temperature increases, the Pd is segregated to the outermost surface of the support and is therefore accessible to the reactants. This phenomenon outweighs the sintering of the metallic particles and explains the unexpected increase in the Pd/C ratio.

As regards the effect of the Al addition, the B.E. of the Pd 3d peak increases from 335.6 eV, corresponding to the sample Pd/BC (800 °C), to 336.1 eV for the sample Pd-Al(7)/BC (800 °C), (see Table 5). This increase in the B.E. indicates a transfer of the electronic charge from the Pd nanoparticles to the Al oxide [37]. Finally, comparing the values of the Al/C ratios in Tables 1 and 5, an enrichment of Al at the surface of the support can also be observed. However, the decrease in the Pd/Al ratios measured at the surface with respect to the bulk composition, see Table 1, indicates that the segregation of the aluminium oxide is more intense than that of the Pd nanoparticles.

Fig. 4 shows the Raman spectra of the three catalysts prepared under different conditions. All the spectra show two broad peaks, one at ca. 1350 cm^{-1}, the D band zone, and another centred at ca. 1590 cm^{-1}, which is called the G band zone. The shape of the two peaks is characteristic of these types of carbonaceous material [38], and their interpretation is quite complex due to the broadness of D and G bands which may be caused by the presence of several structural contributions. Thus, Fig. 5 illustrates the deconvolution in five peaks of the signal obtained for the sample Pd-Al(7)/BC-800 °C, at 75 min. These peaks are associated to the contribution of C=C chain stretching and CH wagging modes (peak 1 at ~1150 cm^{-1}) [39], to the in-plane vibrations of sp2 bonded carbon within structural defects (peak 2 (D) at ~1350 cm^{-1}) [40,41], to the amorphous sp^2 carbon bonded phase (peak 3 at ~1450 cm^{-1}) [42], to the in-plane vibrations of the sp^2-bonded crystallite carbon (peak 4 (G) at ~1580 cm^{-1}) [40,41] and to the disorders resulting from the finite size effect or lattice distortion (peak 5 at ~1620 cm^{-1}) [43,44]. The table inserted in Fig. 5 contains an example of the fitting parameters of the Raman spectra using a Gaussian-Lorentzian mixed function.

Table 6 shows the values of the ratio I_G/I_D, calculated as the intensity ratio between the G (peak 4) and D (peak 2) bands. The parameter L_a and the graphitic fraction (X_G) have been calculated from this ratio. For polycrystalline graphitic materials, the I_G/I_D ratio correlates with the effective crystallite size (L_a), due to the increasing fraction of sp^2 hybridised carbons which contribute to the G band but not to the D band [40,42]. This parameter is calculated by the empirical equation proposed by Tuinstra et al. [45] as $L_a = 4.35 \cdot I_G/I_D$, and subsequently generalized by Pimenta et al. [46]. On the other hand, if it is assumed that the I_G and I_D have the same proportionality coefficient, the graphitic fraction (X_G) can be estimated as: $X_G = I_G/(I_D + I_G)$. Therefore, the deconvolution of the Raman spectra in Fig. 4 allows us to ascertain the influence of the operating conditions during the catalyst preparation on the degree of graphitization or the orientation of the graphite planes, and on the relative amount of defects in the carbonaceous support.

For the Pd/BC catalyst, it is observed that the value of I_G/I_D decreases from 1.70 to 1.02 when the decomposition temperature increases from 600 °C to 800 °C, indicating an increase in the defects and a decrease in the degree of graphitization of the biomorphic carbon formed. The decrease in the graphitic character as the treatment temperature increases could be attributed to the gasification of the carbon formed by the hydrogen included in the synthesis atmosphere. It is further increased by the presence of Pd, which catalyses the support gasification. In contrast, for the samples prepared at 800 °C the addition of Al increases the ratio I_G/I_D, favouring the increase in the effective

Table 4
Influence of thermal decomposition temperature and Al addition on the Pd particle size.

Catalyst	Average Pd diameter (XRD) (nm)	Average Pd diameter (TEM) (nm)	Standard deviation (nm)
Pd/BC (600 °C, 30 min)	5.8	7.4	2.1
Pd/BC (700 °C, 30 min)	12.5	12.1	2.8
Pd/BC (800 °C, 30 min)	30.1	36.4	10.3
Pd-Al(1.75)/BC (800 °C, 30 min)	34.6	32.0	14.1
Pd-Al(7)/BC (800 °C, 30 min)	35.0	34.9	10.2
Pd-Al(7)/BC (800 °C, 75 min)	61.8	59.6	21.5
Pd-Al(7)/BC (800 °C, 120 min)	65.9	64.5	21.0

Table 5
Surface atomic composition obtained from XPS. Decomposition time = 30 min.

Catalyst	C 1s	O 1s	Pd 3d	Al 2p	10^3*Pd/C	10^3*Al/C	Pd/Al
Pd/BC	284.9 eV.	533.7 eV.	335.6 eV.	–	–	–	–
(600 °C)	91.72%	7.57%	0.71%	–	7.74	–	–
Pd/BC	284.9 eV.	532.9 eV.	335.6 eV.	–	–	–	–
(700 °C)	91.51%	7.71%	0.78%	–	8.52	–	–
Pd/BC	284.9 eV.	532.7 eV.	335.6 eV.	–	–	–	–
(800 °C)	90.56%	8.64%	0.80%	–	8.83	–	–
Pd-Al(1.75)/BC	284.9 eV	532.3 eV	335.9 eV	74.9 eV		–	–
(800 °C)	89.58%	8.61%	0.30%	1.51%	3.35	16.9	0.20
Pd-Al(7)/BC	284.9 eV	532.0 eV	336.1 eV	75.1 eV		–	–
(800 °C)	80.72%	15.83%	0.24%	3.25%	2.97	40.3	0.07
Pd-Al(7)/BC	284.9 eV	532.1 eV	336.2 eV	75.1 eV			
(800 °C)[a]	79.24%	17.08%	0.26%	3.42%	3.28	43.2	0.08

[a] Thermal treatment duration: 75 min.

crystalline size and in the degree of graphitization. However, the augmentation of the decomposition time of the *Pd-Al(7)/BC* catalyst seems to decrease the graphitic character of the support.

In order to ascertain how the decomposition temperature and the Al addition affect the external structure of these carbonaceous materials, the catalysts were also analysed by SEM. In the images in Fig. 6 show that the external shape of the cellulose remains in the biomorphic carbon after the synthesis process, presenting a very smooth surface typical of these types of carbonized material [47].

The samples which decomposed at 600 °C and 700 °C (Fig. 6a and b) exhibit a similar structure. However, the morphology of the catalyst which decomposed at 800 °C (Fig. 6c) is quite different, showing a larger number of holes opened in the external surface. In addition, the sample which decomposed at 600 °C (Fig. 6a) does not present visible metallic particles on the external surface, the sample prepared at 700 °C (Fig. 6b) shows a small amount of these particles, whereas at 800 °C (Fig. 6c) the image shows a large amount of Pd nanoparticles. This was corroborated by EDX measurements (not shown). Therefore, the increase in the decomposition temperature during the catalyst preparation not only increases the average size of the Pd particles, but also releases these particles from the carbon matrix to the external surface of the catalysts, greatly influencing their catalytic activity. Fig. 6d and e corresponds to the catalyst containing 1.75% and 7% of Al, respectively. The external macrostructure observed in both cases is similar to the Pd/BC samples, the Pd particles also being clearly visible. The alumina particles formed are not visible by SEM due to their small size.

Fig. 7 shows the TEM images and the Pd particle size distribution obtained from them for the synthesised catalysts. The Pd particle size distribution and the average diameter of the Pd particles were calculated with a number greater than 500 particles, which confers an important statistical relevance. In addition, owing to the shape of the Pd particle size distributions obtained, it was decided to calculate the average diameter of the Pd particles using the following expression [48]: $\overline{d_p} = \sum (n_i \cdot d_i^3) / \sum (n_i \cdot d_i^2)$. In this equation $\overline{d_p}$ is the average diameter of Pd particles and n_i the number of particles with d_i diameter. For the samples prepared without Al, after preparation at 600 and 700 °C, the catalyst has a high dispersion of Pd particles (Fig. 7a and b) presenting narrow distributions of 7.4 ± 2.1 nm and 12.1 ± 2.8 nm, respectively. In both cases, the distributions have an incipient tail that accounts for small amounts of larger particles up to ca. 13–15 nm for 600 °C and ca. 21–22 nm for 700 °C. In contrast, the catalyst prepared at 800 °C, see Fig. 7c, shows lower Pd dispersion and a broad non-symmetric particle size distribution. In this case, small particles are observed (ca. 5 nm), and also large particles larger than 30 nm. The average particle size is 36.4 ± 10.3 nm.

Fig. 7d–g shows the TEM images for the Pd-Al/BC catalysts prepared at 800 °C with 1.75% and 7% of Al, respectively, while increasing the time of decomposition. As shown in the SEM pictures, Fig. 6, the addition of the Al does not seem to modify the smooth surface of the support. However, in all the samples with Al the structure of the carbonaceous support formed by the slit-type pores that make up the graphenic structures formed during the preparation of the catalyst can

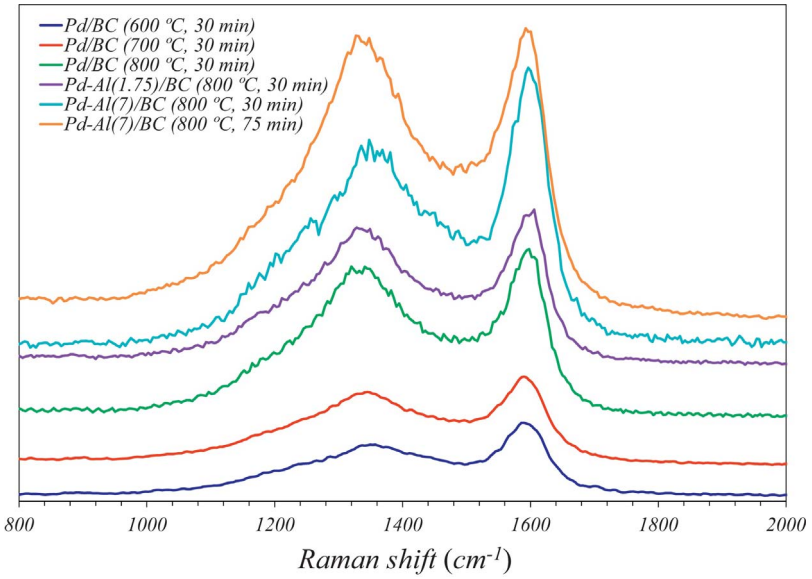

Fig. 4. Raman spectra obtained for prepared catalysts. Influence of thermal decomposition temperature and time, and aluminium addition.

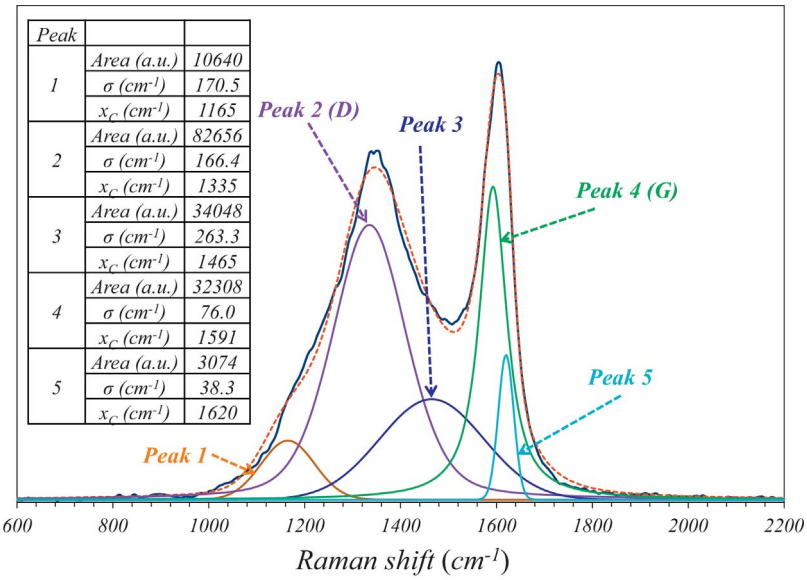

Peak		
1	Area (a.u.)	10640
	σ (cm-1)	170.5
	xC (cm-1)	1165
2	Area (a.u.)	82656
	σ (cm-1)	166.4
	xC (cm-1)	1335
3	Area (a.u.)	34048
	σ (cm-1)	263.3
	xC (cm-1)	1465
4	Area (a.u.)	32308
	σ (cm-1)	76.0
	xC (cm-1)	1591
5	Area (a.u.)	3074
	σ (cm-1)	38.3
	xC (cm-1)	1620

Fig. 5. Deconvolution of Raman signal obtained for Pd-Al(7)/BC catalyst prepared at 800 °C during 75 min. Embedded table shows the deconvolution results of the spectrum.

be clearly observed.

Fig. 7c–e corresponds to the samples prepared during 30 min at 800 °C, with increasing amounts of Al (0, 1.75 and 7% respectively). Although the average diameter of the Pd particles does not seem to vary, the size distributions change. A bimodal distribution appears with quite a large fraction of Pd particles of large diameter. If the time of thermal decomposition is increased to 75 and to 120 min, Fig. 7f and g, the particle size increases dramatically from 34.9 ± 10.2 nm at 30 min to 64.5 ± 21.0 nm at 120 min, see Table 4. The increase in the time of decomposition also strongly modifies the size distribution. After 75 and 120 min, see Fig. 7f and g, the distributions are much broader, being almost monomodal, and centred at increased values. Clearly, the sintering of the Pd particles is intensified at increasing times of decomposition, and consequently a large number of the particles have large diameters.

Fig. 8a–d shows the combined results of STEM-HAADF and energy-dispersive X-ray spectroscopy (EDS) of the Pd-Al(7)/BC catalyst prepared at 800 °C during 75 min. The EDS spectra of area 1 (Fig. 8b) shows a high content in carbon and Al. The EDS spectra of area 2 (Fig. 8c), which corresponds mainly to a Pd nanoparticle, shows the peaks corresponding to the Pd. The presence of carbon and Al due to the part of the area that is not covered by the Pd nanoparticle is also detected. Finally, Fig. 8d shows the EDS spectra of the single point of the biomorphic carbon surface. The results indicate that the main component of this point is carbon and that a minor amount of Al is detected. These results seem to indicate that the Pd/Al ratios change considerably over the surface, developing a low degree of interaction between both components. Obviously the XPs results give an average value of these Pd/Al ratios.

Table 7
Conversion and TOF during cyclohexene hydrogenation. Reaction time: 1 h.

Catalyst	Cyclohexene conversion (%)	Pd dispersion (%)	TOF (s^{-1})
Pd(1%)/SiO_2	17.8	16.6	10.2
Pd/BC (600 °C, 30 min)	0.2	15.0	–
Pd/BC (700 °C, 30 min)	1.5	9.2	0.9
Pd/BC (800 °C, 30 min)	10.7	3.1	2.9
Pd-Al(1.75)/BC(800 °C, 30 min)	14.1	3.5	3.1
Pd-Al(7)/BC (600 °C, 30 min)	1.4	17.3	0.1
Pd-Al(7)/BC (600 °C, 75 min)	1.3	15.6	0.1
Pd-Al(7)/BC (600 °C, 120 min)	4.1	8.1	0.5
Pd-Al(7)/BC (700 °C, 30 min)	13.5	3.2	2.9
Pd-Al(7)/BC (800 °C, 30 min)	16.4	3.2	4.8
Pd-Al(7)/BC (800 °C, 75 min)	29.7	1.9	11.9
Pd-Al(7)/BC (800 °C, 120 min)	23.6	1.7	9.5

3.2. Catalytic behaviour

The biomorphic carbon-based catalysts were tested in the liquid

Table 6
I_G/I_D, L_a and X_G parameters calculated from the deconvolution results of the Raman signals obtained for Pd/CB and Pd-Al/CB catalysts. Influence of thermal decomposition temperature and aluminium addition. Decomposition time = 30 min.

Temperature					
600 °C	700 °C	800 °C	800 °C	800 °C	800 °C
	% Aluminium				
	0.00	0.00	0.00	1.75	7.00	7.00[a]
I_G/I_D	1.70	1.28	1.02	1.04	1.14	0.92
L_a (nm)	7.40	5.58	4.43	4.51	4.96	3.98
X_G	0.63	0.56	0.50	0.51	0.53	0.48

[a] Catalyst prepared during 75 min.

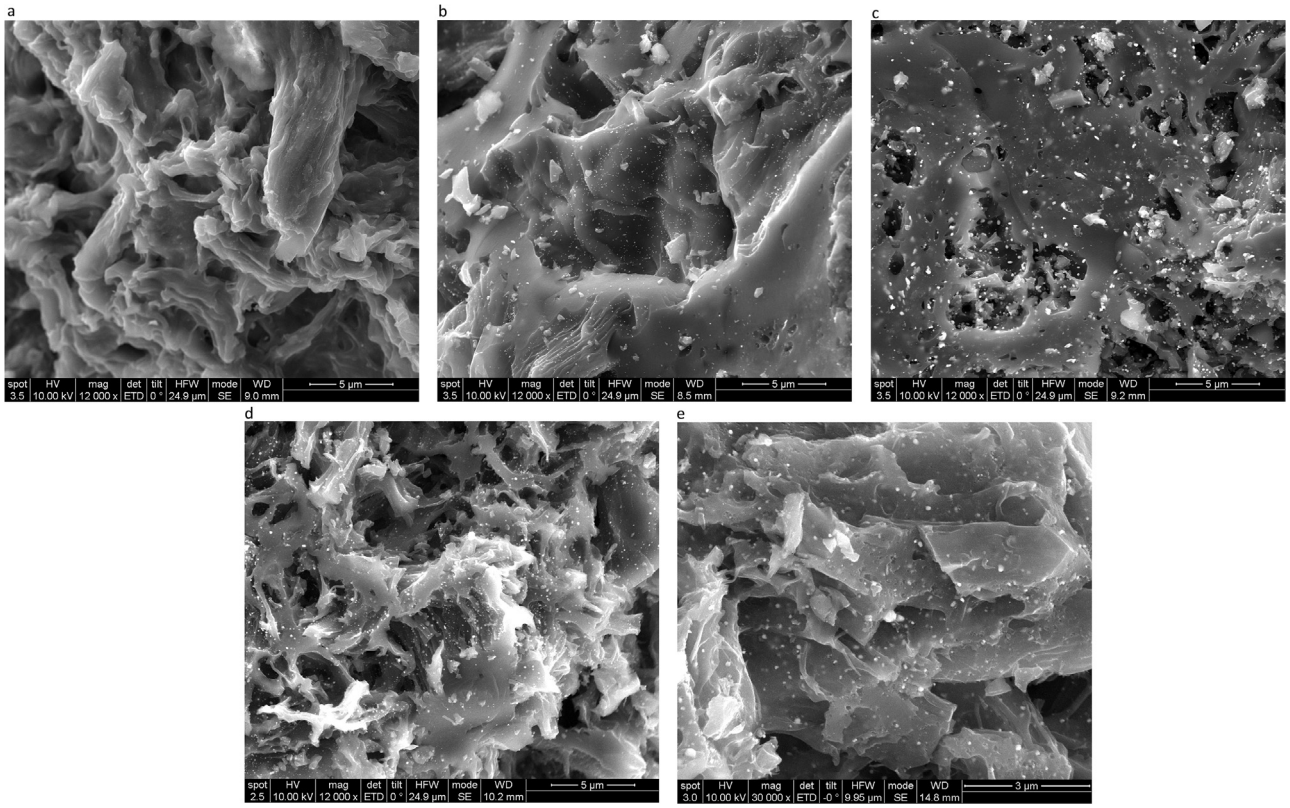

Fig. 6. SEM images of Pd/BC catalysts prepared at: a) 600 °C, b) 700 °C, c) 800 °C, d) Pd-Al(1.75)/BC at 800 °C, e) Pd-Al(7)/BC at 800 °C. Decomposition time = 30 min.

phase hydrogenation of cyclohexene at 100C. Preliminary experiments carried out under increasing values of the stirring rate and decreasing values of the particle support allows the selection of kinetic control operating conditions where there is a negligible influence of external and internal mass transfer limitations. In addition, the experiment carried out with the Pd-Al(7)/BC catalyst was repeated and the error calculated for the cyclohexene conversion was below 3%. The values of the reaction rates, taken to calculate the turnover frequency (TOF) for each catalyst, were calculated after 1 h of reaction given that in this period a linear increase the conversion was observed. The reaction rate was therefore kept constant and the reactor operated under differential conditions.

Table 7 shows the values obtained for the conversion of cyclohexene, the percentage of Pd nanoparticle dispersion, and the TOF (s^{-1}) calculated for each catalyst prepared. The TOF is defined as the number of cyclohexene moles consumed during the reaction per atom of exposed Pd per second. To calculate the TOF value, first it is necessary to know the Pd dispersion obtained in each sample. The dispersion was calculated following the expression [48]: $D_M = (V_M/A_M)\cdot(6/\overline{d_p})$. In this equation D_M is the metallic dispersion, V_M is the volume occupied by a bulk metal atom, A_M is the area per metal atom and $\overline{d_p}$ is the mean particle size, calculated by TEM measurements. For a Pd particle, V_M is 0.0147 nm^3 and A_M is 0.07933 nm^2 [48]. The table also includes the results obtained with a Pd(1%)/SiO_2 catalyst with 16.6% metal dispersion for the purposes of comparison. This catalyst presents a TOF of 10.2 s^{-1}.

The results shown in Table 7 indicate that the values of the catalytic activity obtained with the Pd/BC catalyst prepared at 600 °C and 700 °C are very low in spite of the higher values of Pd dispersion attained in these catalysts. Surprisingly, for the catalyst synthesized at 800 °C, which has a lower Pd dispersion, the activity increases reaching a cyclohexene conversion of 10.7%, corresponding to a TOF of 2.9 s^{-1}. As regards the Al containing catalysts, the Pd-Al(1.75)/BC and Pd-Al (7)/BC catalysts with similar low Pd dispersions present increasing TOF values, reaching a value of 4.8 s^{-1} for the sample with 7% of Al. In addition, as with the catalysts that do not contain Al, the activity of the Pd-Al(7)/BC catalysts is increased with the decomposition temperature.

Although it is well known that the hydrogenation of cyclohexene is "structure insensitive" [49], and therefore the intrinsic activity of the catalysts should not vary with the particle size, these results indicate that the Pd dispersion is not the most important parameter in this type of catalyst. This is confirmed by studies of samples prepared at increasing decomposition times, 75 and 120 min [6,50]. In these cases, the Pd dispersion decreases until reaching values as low as 1.9 and 1.7%. Nevertheless, the TOF substantially increases up to 11.9 and 9.5 s^{-1}, respectively. These values are comparable to the value obtained with the Pd(1%)/SiO_2 catalyst, which has a 16.6% of Pd dispersion. This unforeseen result can be explained considering the data in Tables 2 and 4, referring to the texture and Pd dispersion of the catalysts. Thus, the more active catalysts are those with the larger Pd particles. In contrast, the less active Pd/BC catalysts with almost negligible conversions have Pd dispersions comparable to that obtained with the Pd(1%)/SiO_2. These catalysts, obtained after preparation at low temperatures (e.g. 600 °C), are inactive because the smaller Pd particles formed are trapped in the internal structure of the micropores of the support and/or embedded inside the carbon matrix. Considering that the kinetic diameter of cyclohexene is ca. 0.6 nm [51], both factors can explain the low activity observed in this case. In contrast, after decomposition at 800 °C, the larger Pd particles formed are situated on the external surface of the catalyst, being accessible to the reactants. This explains the observed increase in activity. In addition, the formation of holes in the catalyst through carbon gasification could also contribute to the high hydrogenation activity of the catalysts generated at high temperature (i.e. 800 °C). At this temperature, the diameter of the pores is enlarged leading to the formation of a composite with a hierarchical structure and therefore with high diffusion rate efficiency.

All the catalytic results obtained are summarized in Fig. 9. This log-

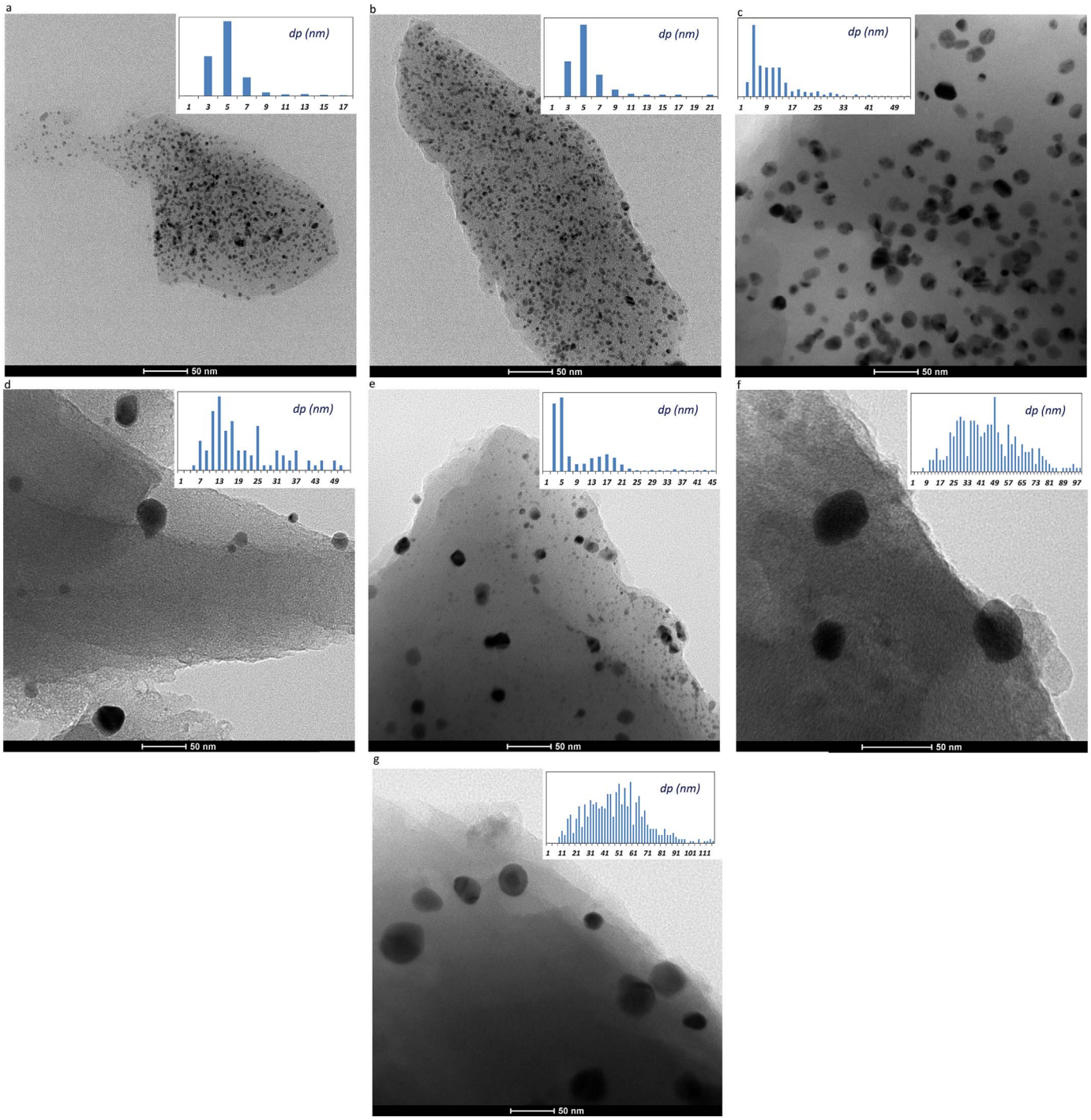

Fig. 7. TEM images and Pd particle size distribution for Pd/BC catalysts prepared at: a) 600 °C, b) 700 °C and c) 800 °C during 30 min, d) Pd-Al(1.75)/BC prepared at 800 °C during 30 min, and Pd-Al(7)/BC prepared at 800 °C during e) 30 min, f) 75 min and g) 120 min.

log figure represents the evolution of the TOF vs. the average particle size for each catalyst tested. The activity obtained with the Pd/SiO2 (red line) is taken as the reference for the intrinsic activity. In the case of the catalysts supported on the biomorphic carbon, the same intrinsic activity is only obtained with the more sintered catalysts, which have average Pd particle sizes of around 60 nm. For the rest of the catalysts, the decrease in activity is quite dramatic as a consequence of the above-mentioned diffusional limitations. Interestingly, the power-law dependence between the TOF of the BC catalysts with their average Pd diameter, ($TOF \sim (d_{p,Pd})^2$), can also be used to predict the catalyst activity for a given sample.

Furthermore, as has been mentioned, the addition of Al to the catalyst produces an increase in the catalytic activity. This improvement is directly related to the transfer of an electronic charge from the Pd nanoparticles to the Al oxide [37], observed by XPS (see Table 5). This phenomenon modifies the adsorption properties of the metal. This change in the reactivity of the cyclohexene can be observed in Table 7. Thus, the CE conversion increases from 10.7% obtained with the catalyst Pd/CB (800 °C, 30 min) to 14.1% for the Pd-Al(1.75)/CB (800 °C, 30 min) and to 16.4% for the Pd-Al(7)/CB (800 °C, 30 min).

Finally, in order to have fuller information about the catalytic performance of the catalyst Pd-Al(7)/BC (800 °C, 75 min) Fig. 10 shows the influence of the hydrogen partial pressure and of the reaction temperature on the TOF. The value obtained for the kinetic order with

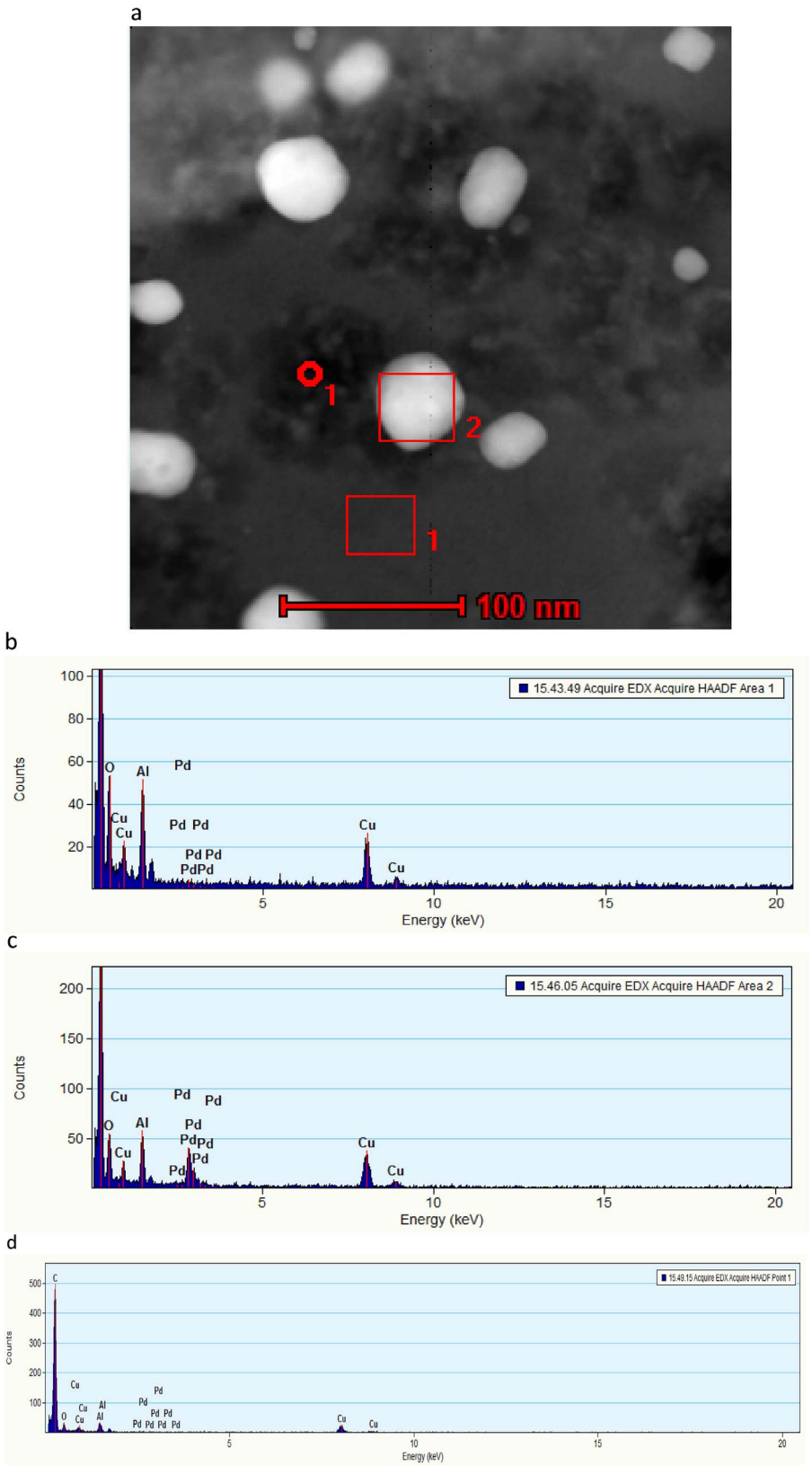

Fig. 8. a) STEM-HAADF micrograph of Pd-Al(7)/BC catalyst prepared at 800 °C during 75 min. EDS spectrum of b) area 1, c) area 2, d) single point O_1.

respect to H_2 (m = 0.76) is consistent with a reaction mechanism in which the rate-determining step is the first hemi-hydrogenation of the adsorbed cyclohexene molecule [49,52]. In addition, the apparent activation energy calculated, 42 kJul/mol, is similar to the previous results, confirming also the absence of the diffusional limitations.

4. Conclusions

The thermal decomposition of cellulose impregnated with metallic precursors under a reductive atmosphere is an easy and appropriate method for preparing catalysts based on biomorphic carbons. The Pd

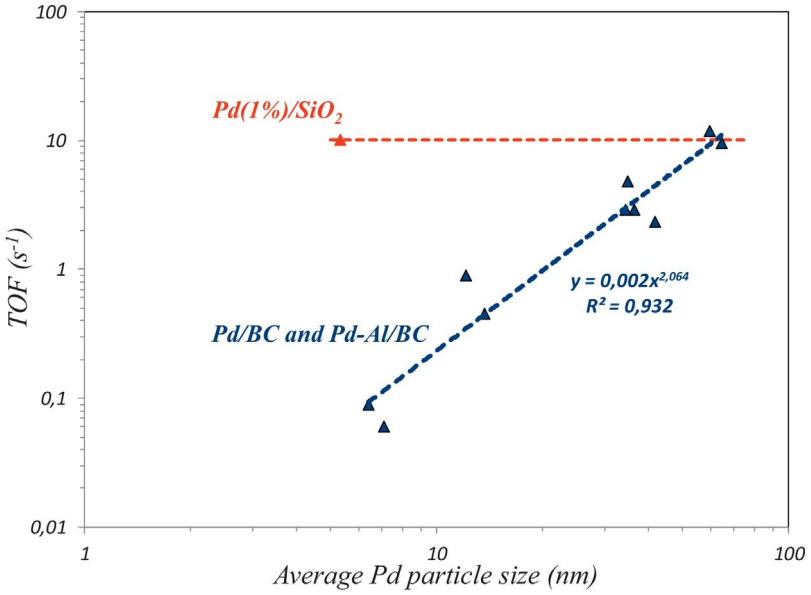

Fig. 9. TOF (s^{-1}) vs. average Pd nanoparticle size.

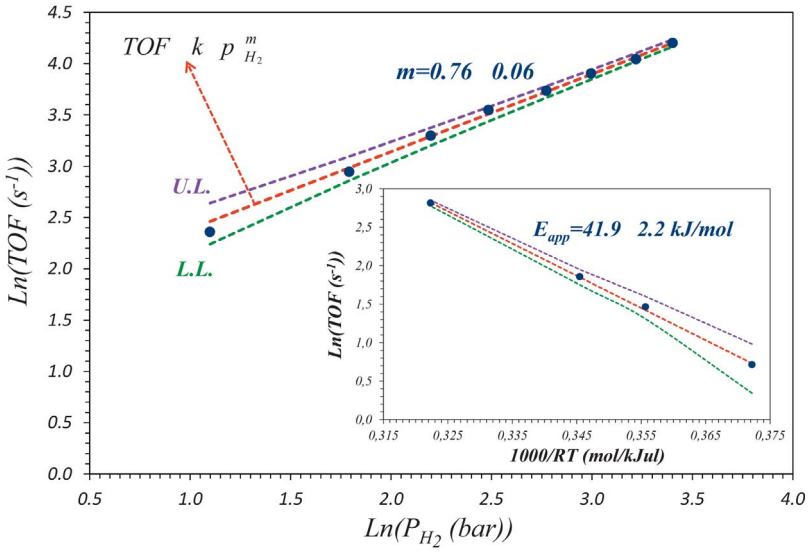

Fig. 10. Effect of hydrogen partial pressure on the TOF (s^{-1}) and Arrhenius plot for the liquid-phase hydrogenation of cyclohexene.

and Pd-Al/BC catalysts obtained by this method have a suitable structure and properties for use in liquid-phase hydrogenation reactions.

The characterisation results indicate that the carbonaceous supports prepared in this way have a high microporosity (up to 97% micropore volume) and BET surface values up to 470 m^2/g, while maintaining the original external morphology.

The textural characterization results have revealed a linear relationship between the BET surface area and the micropore volume. The slope of this line is 2659.2 m^2/cm^3, which is similar to that of other synthetic carbons obtained by thermal treatments. This unexpected result can be used to predict the effect of the synthesis conditions on the textural properties.

The use of low temperatures (ca. 600 °C) during the decomposition step allows the preparation of highly dispersed catalysts, with narrow Pd particle size distributions of 5–7 nm. However, in this case, the catalyst is almost inactive because the particles are confined in the internal structure of the micropores and/or embedded inside the carbon matrix, being almost unreachable by the molecules of the reactants.

On the other hand, the decomposition at elevated temperatures (ca. 800 °C) increases the Pd particle size due to sintering, attaining values of around 40–60 nm. This phenomenon is enhanced with the decomposition time, although it is not affected by the presence of Al. In spite of this large size, the catalyst obtained is clearly more active because the Pd particles are left exposed on the external surface of the carbonaceous support, being accessible to the cyclohexene molecules. In addition, the presence of Al favours the cyclohexene conversion due to the enhancement of the adsorption on the Pd surface as a consequence of a charge transfer phenomenon.

The results of this study have led to the development of guidelines for the preparation of catalysts based on raw lignocellulosic materials with the aim of maximising their catalytic performance.

Acknowledgements

The authors acknowledge financial support from MINECO (Madrid, Spain)-FEDER, Projects CTQ2010-16132 and ENE2013-47880-C3-1-R. The authors would like to thank Dr. Víctor Sebastián, Dr. Silvia Irusta

and Adrián Ramírez for their TEM, XPS and SEM measurements.

References

[1] A.G. Pandolfo, A.F. Hollenkamp, J. Power Sources 157 (2006) 11–27.
[2] L. Zhang, X.S. Zhao, Chem. Soc. Rev. 38 (2009) 2520–2531.
[3] B. Fang, H. Zhou, I. Honma, J. Phys. Chem. B 110 (10) (2006) 4875–4880.
[4] C.K. Leong, D.D.L. Chung, Carbon 42 (11) (2004) 2323–2327.
[5] C. Moreno-Castilla, F.J. Maldonado-Hodar, Carbon 43 (3) (2004) 455–465.
[6] F. Cazaña, M.T. Jimaré, E. Romeo, V. Sebastián, S. Irusta, N. Latorre, C. Royo, A. Monzón, Catal. Today 249 (2015) 127–136.
[7] L. Shia, P. Zhu, R. Yang, X. Zhang, J. Yao, F. Chen, X. Gao, P. Ai, N. Tsubaki, Catal. Comm. 89 (2017) 1–3.
[8] T.X. Fan, S.K. Chow, D. Zhang, Prog. Mater. Sci. 54 (2009) 542–659.
[9] J. Will, C. Zollfrank, A. Kaindl, H. Sieber, P. Greil, Keram. Z. 62 (2010) 114–120.
[10] B. Bhrushan, Philos. Trans. R. Soc. A 367 (2009) 1445–1486.
[11] S. Zhu, D. Zhang, Z. Li, H. Furukawa, Z. Chen. Langmuir 24 (2008) 6292–6299.
[12] L. Sapei, R. Noeske, P. Strauch, O. Paris, Chem. Mater. 20 (2008) 2020–2025.
[13] A. Al-Sawalmih, C. Li, S. Siegel, P. Fratzl, O. Paris, Adv. Mater. 21 (2009) 4011–4015.
[14] H.O. Fabritius, C. Sasch, P.R. Triguero, D. Raabe, Adv. Mater. 21 (2009) 391–400.
[15] O. Paris, I. Burgert, P. Fratzl, MRS Bull. 35 (2010) 219–225.
[16] G. Fritz-Popovski, D. Van Opdenbosch, C. Zollfrank, B. Aichmayer, O. Paris, Adv. Func. Mater 23 (2013) 1265–1272.
[17] L.J. Gibson, Metals Mater. 8 (1992) 333–338.
[18] P. Greil, J. Eur. Ceram. Soc. 21 (2001) 105–118.
[19] H. Sieber, A. Mater Sci Eng, 412 (2005) 43–47.
[20] Y.S. Shin, J. Liu, J.H. Chang, Z.M. Nie, G. Exarhos, Adv. Mater 13 (2001) 728–732.
[21] Z.T. Liu, T.X. Fan, W. Zhang, D. Zhang, Microporous Microporous Mater. 85 (2005) 82–88.
[22] M.M. Dubinin, L.V. Radushkevich, Proc. Acad. Sci. USSR 55 (1947) 331–333.
[23] X. Xie, B. Goodell, D. Zhang, D.C. Nagle, Y. Qian, M.L. Peterson, J. Jellison, Bioresour. Technol. 100 (2009) 1797–1802.
[24] M. Zwinkels, S. Jaras, P. Menon, T. Griffin, Catal. Rev. Sci. Eng. 35 (1993) 319–358.
[25] M. Peuckert, J. Phys. Chem. 89 (1985) 2481–2486.
[26] F. Rodriguez-Reinoso, A. Sepulveda-Escribano, Carbon as catalyst support, in: Ph. Serp, J.L. Figueiredo (Eds.), Carbon Materials for Catalysis, John Willey and sons, USA, New Jersey, 2009.
[27] J.H. Bitter, K.P. de Jong, Preparation of carbon-supported metal catalysts, in: P. Serp, J.L. Figueiredo (Eds.), Carbon Materials for Catalysis, John Willey and sons, New Jersey, USA, 2009.
[28] K.S.W. Sing, D.H. Everett, R.A.W. Haul, L. Moscou, R.A. Pierotti, J. Rouquerol, T. Siemieniewska, Pure Appl. Chem. 57 (1985) 603–619.
[29] S. Lowell, J. Shields, M.A. Thomas, M. Thommes, Characterization of Porous Solids and Powders: Surface Area Pore Size and Density, Springer, The Netherlands, Dordrecht, 2006.
[30] C. Scherdel, G. Reichenauer, M. Wiener, Microporous Microporous Mater. 132 (2010) 572–575.
[31] M. Wiener, G. Reichenauer, T. Scherb, J. Fricke, J. Non Cryst. Solids 350 (2004) 126–130.
[32] M. Wiener, G. Reichenauer, F. Hemberger, H.P. Ebert, Int. J. Thermophys. 27 (2006) 1826–1843.
[33] S. Brunauer, P.H. Emmett, E. Teller, J. Am. Chem. Soc. 60 (2) (1938) 309–319.
[34] R. Pirard, J.P. Pirard, Récents Prog. Génie. Procédés 15 (2001) 149–159.
[35] F. Noville, C. Gommes, C. Doneux, A. Brasseur, R. Pirard, J.P. Pirard, Stud. Surf. Sci. Catal. 144 (2002) 419–426.
[36] D.P. Serrano, J.A. Botas, J.L.G. Fierro, R. Guil-Lopez, P. Pizarro, G. Gomez, Fuel 89 (2010) 1241–1248.
[37] B. Ealet, E. Gillet, Surf. Sci. 367 (1996) 221–230.
[38] Y.-R. Rhim, D. Zhang, D.H. Fairbrother, K.A. Wepasnick, K.J. Livi, R.J. Bodnar, D.C. Nagle, Carbon 48 (2010) 1012–1024.
[39] A. Ferrari, J. Robertson, Phys. Rev. B 63 (2001) 121405-1-121405-4.
[40] A. Ferrari, J. Robertson, B. Phys Rev, 61 (2000) 14095–14107.
[41] M.S. Dresselhaus, A. Jorio, M. Hofmann, G. Dresselhaus, R. Saito, Nano Lett. 10 (2010) 751–758.
[42] T. Jawhari, A. Roid, J. Casado, Carbon 33 (1995) 1561–1565.
[43] P. Lespade, R. Al-Jishi, M.S. Dresselhaus, Carbon 20 (1982) 427–431.
[44] D.G. McCulloch, S. Prawer, A. Hoffman, Phys. Rev. B 50 (1994) 5905–5917.
[45] F. Tuinstra, J. Koenig, J. Chem. Phys. 53 (1970) 1126.
[46] M.A. Pimenta, G. Dresselhaus, M.S. Dresselhaus, L.G. Cancado, A. Jorio, R. Saito, Phys. Chem. Chem. Phys. 9 (2007) 1276–1291.
[47] L. Ma, X. Zhang, D. Lin, Y. Chun, Q. Xu, Appl. Catal. A 460–461 (2013) 26–35.
[48] G. Bergeret, P. Gallezot, G. Ertl, H. Knözinger, J. Weitkamp (Eds.), Handbook of Heterogeneous Catalysis, vol. 3, Wiley-VCH, Weinheim, 1997, p. 738.
[49] E.E. Gonzo, M. Boudart, J. Catal. 52 (1978) 462–471.
[50] F. Cazaña, M.T. Jimaré, C. Royo, E. Romeo, N. Latorre, A. Monzón, Proceedings of 4th International Workshop UBIOCHEM IV: Utilization of Biomass for Sustainable Fuels and Chemicals, Valencia (Spain) 14th–16th October, 2013.
[51] M. Niwa, Y. Kawashima, Y. Murakami, J. Chem. Soc. Farad. Trans. 1 (81) (1985) 2757–2761.
[52] B.Y. Lee, Y. Inoue, I. Yasumori, Bull. Chem. Soc. Jpn. 54 (1981) 13–19.